Economical and effective sulfide catalysts for dye-sensitized solar cells as counter electrodes

PCCP

COMMUNICATION

Economical and effective sulfide catalysts for dye-sensitized solar cells as counter electrodes†

Mingxing Wu,[a] Yudi Wang,[a] Xiao Lin,[a] Naisen Yu,[b] Liang Wang,[a] Linlin Wang,[a] Anders Hagfeldt[c] and Tingli Ma*[a]

Molybdenum sulfide (MoS$_2$) and tungsten sulfide (WS$_2$) are proposed as counter electrode (CE) catalysts in a I$_3^-$/I$^-$ and T$_2$/T$^-$ based dye-sensitized solar cells (DSCs) system. The I$_3^-$/I$^-$ based DSCs using MoS$_2$ and WS$_2$ CEs achieved power conversion efficiencies of 7.59% and 7.73%, respectively.

Because of the efforts in the past two decades, remarkable advances in dye-sensitized solar cells (DSCs) have been achieved.[1,2] However, despite their advantages, such as simple fabrication procedure, good plasticity, and environmental friendliness, DSCs are limited by several problems, such as low power conversion efficiency (PCE), high cost, and poor stability. These should be addressed before they can be applied at a commercial level. Previous studies mainly focused on designing low-cost sensitizers or electrical conductive substrates to overcome the high cost of DSCs.[3,4] While exploring commercial counter electrode catalysts is a promising way to replace the expensive Pt CE catalyst. This can lead to the reduction of the cost of DSCs. Since 1996, carbon materials have been used as CE catalysts in DSCs.[5,6] In order to develop flexible DSCs, conductive polymers (polypyrrole, and polyaniline) were used as CE catalysts.[7,8] It was found that some inorganic materials such as CoS, TiN, NiN, NiS, WC, MoC, MoO$_2$, WO$_2$, Mo$_2$N, and W$_2$N can be used as CE catalysts. Utilizing these materials resulted in a decent catalytic activity for triiodide reduction or disulfide (T$_2$) reduction.[9–17] Compared to carbon or polymer materials, inorganic materials have unique properties such as material diversity, abundance, low cost, high catalytic activity, and ease of modification.

To date, there have been no reports on the application of MoS$_2$ and WS$_2$ as CE catalysts in DSCs, although MoS$_2$ and WS$_2$ have been applied in the fields of lubricants, refractories, and H$_2$ evolution.[18–22] Molybdenum and tungsten carbides,
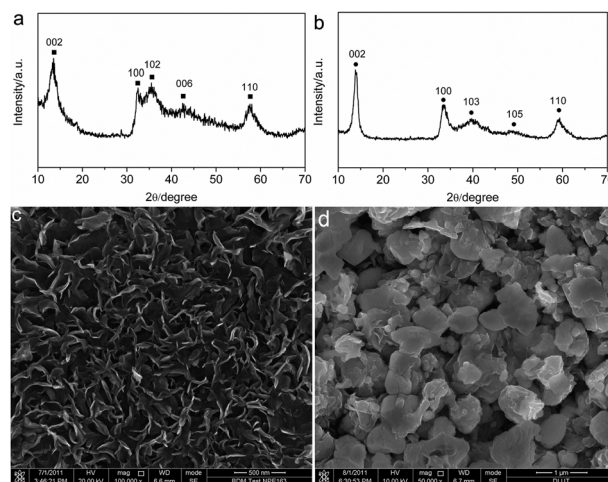
[a] State Key Laboratory of Chemicals, School of Chemical Engineering, Dalian University of Technology, Dalian, China. E-mail: tinglima@dlut.edu.cn; Fax: +86-411-84986230; Tel: +86-411-84986237
[b] Institute of Optoelectronic Technology, School of Physics and Material Engineering, Dalian Nationalities University, Dalian, China
[c] Department of Physical and Analytical Chemistry, Uppsala University, Box 259, SE-751 05 Uppsala, Sweden
† Electronic supplementary information (ESI) available: Details of electrodes fabrication, cells assembly and measurements. See DOI: 10.1039/c1cp22819f

Fig. 1 XRD patterns of (a) MoS$_2$ and (b) WS$_2$; SEM image of (c) MoS$_2$ and (d) WS$_2$.

nitrides, and oxides provide good catalytic behavior in DSCs. Similarly, their sulfides are expected to have the same function due to their high catalytic activity, thermal and chemical stability. In the current work, MoS$_2$ and WS$_2$ were synthesized using a simple chemical method and were used, for the first time, as CE catalysts in DSCs. Fig. 1a and b show the XRD patterns of the synthesized MoS$_2$ and WS$_2$ which are in agreement with the PDF 2 database (MoS$_2$: 75-1539; WS$_2$: 84-1398). The SEM image of the MoS$_2$, as shown in Fig. 1c, exhibits the form of twisted leaves interlocked with each other. On the other hand, the SEM image of WS$_2$, as shown in Fig. 1d, presents the form of accumulated irregular particles piled up with WS$_2$ slices.

Cyclic voltammetry (CV) is widely used in investigating the catalytic activity of a catalyst in previous research.[23] CV was carried out using MoS$_2$, WS$_2$, and Pt as work electrodes. Typically, there are two pairs of redox peaks in the cyclic voltammogram. The left pair can be assigned to the redox reaction represented by eqn (1) and the right pair can be assigned to the redox reaction represented by eqn (2). As shown in Fig. 2a, the cyclic voltammograms of MoS$_2$, WS$_2$, and Pt all show two typical pairs of redox peaks. The CV profile and the peak positions of MoS$_2$, WS$_2$ are similar to Pt's, which indicates similar catalytic
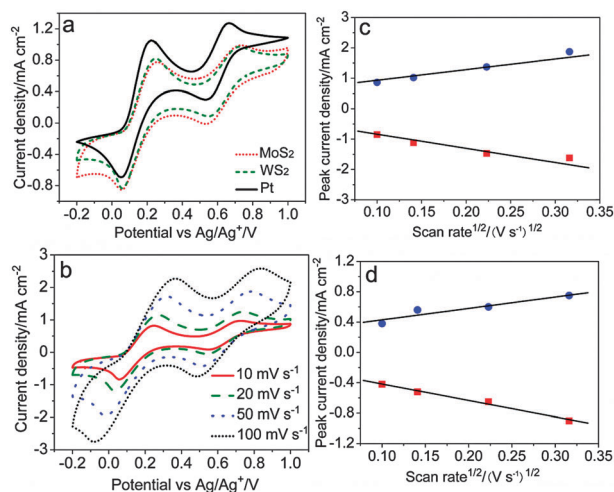
Fig. 2 (a) Cyclic voltammograms of the MoS_2, WS_2, and Pt electrodes for iodide species, scanning rate: 10 mV s^{-1}; (b) cyclic voltammograms of the MoS_2 electrode at various scan rates; relationship of the current densities of anodic (■) and cathodic (●) peaks for (c) redox reaction (1) and (d) redox reaction (2) with the square root of the scan rate.

activities and catalytic mechanism for the triiodide reduction. Fig. 2b shows the cyclic voltammograms of MoS_2 at various scan rates. The current density increases with the increase in the scan rate. Fig. 2c and d show the relationship between the peak current density and the square root of the scan rate, which is in good agreement with eqn (3). As the scan rate increases, the diffusion layer becomes thinner and the electrochemical polarization becomes larger which leads to high overpotential and poor reversibility. The linear relationship indicates the diffusion limitation of cathodic and anodic reactions may affect the transport of the iodide species on the sulfide electrode surfaces.[24] This phenomenon has been observed in an earlier research.[25] Thus, in order to identify the real chemical reaction mechanism, the CV experiments should be performed at low scan rates. CV results show that the MoS_2 and WS_2 are promising catalysts for triiodide reduction and are expected to perform well in I_3^-/I^- based DSCs as CEs.

$$I_3^- + 2e^- \leftrightarrows 3I^- \qquad (1)$$

$$3I_2 + 2e^- \leftrightarrows 2I_3^- \qquad (2)$$

$$i_p = 2.69 \times 10^5 n^{3/2} A D^{1/2} V^{1/2} C \qquad (3)$$

where i_p is the peak current density, n is the number of electrons transferred, A is the area of the electrode, D is the diffusion coefficient, V is the scan rate, and C is the concentration.

Fig. 3 shows the photocurrent density–voltage (J–V) curves of the DSCs using MoS_2, WS_2, and Pt CEs. The photovoltaic parameters are summarized in Table 1. When MoS_2 and WS_2 are used as CEs, the DSCs yield high fill factors (FF) of 0.73 and 0.70, respectively, indicating high catalytic activities for triiodide reduction. The high PCEs of 7.59% and 7.73% are obtained for MoS_2-DSC and WS_2-DSC, respectively, which can match the photovoltaic performance of the DSC (7.64%) using a Pt CE. In addition, the MoS_2-DSC and WS_2-DSC both yield a relatively high open circuit voltage (V_{oc}, > 0.75 V) and short circuit current density (J_{sc} of approximate 14 mA cm^{-2})
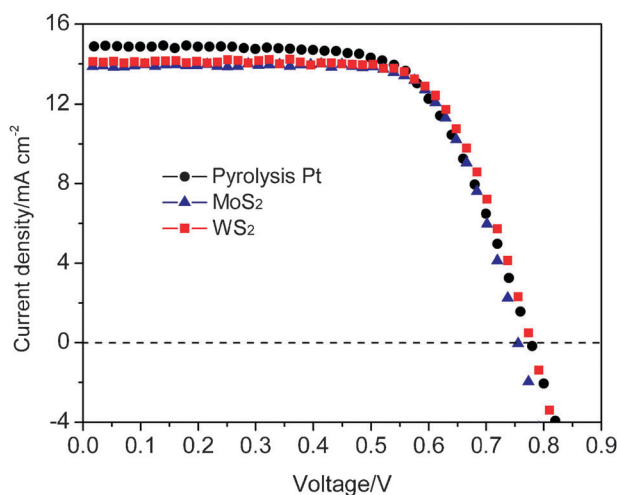

Fig. 3 Photocurrent density–voltage (J–V) curves of the DSCs using MoS_2 (▲), WS_2 (■), and Pt CEs (●).

Table 1 Photovoltaic parameters of the DSCs using MoS_2, WS_2 and Pt CEs and EIS parameters of the dummy cells fabricated with two identical MoS_2, WS_2 and Pt electrodes

Sample	V_{oc}/V	J_{sc}/mA cm^{-2}	FF	η (%)	R_s/Ω	R_{ct}/Ω	C_μ/μF	Z_N/Ω
Pt	0.78	14.89	0.66	7.64	12.7	3.0	2.1	9.5
MoS_2	0.76	13.84	0.73	7.59	20.8	0.5	134.1	231.9
WS_2	0.78	14.13	0.70	7.73	19.4	0.3	198.0	181.4

compared to the Pt-DSC. The J–V performance shows that MoS_2 and WS_2 are impressive CE catalysts for I_3^-/I^- based DSCs.

To detect the electrochemical process on the two sulfide electrodes for iodide species, electrochemical impedance spectroscopy (EIS) was performed using symmetrical cells (SCs) fabricated with two identical CEs clipping the electrolyte. Fig. 4a shows the Nyquist plots of the MoS_2 and WS_2 based SCs. Inset A is an equivalent circuit diagram and Inset B is the Nyquist plot of the Pt-SC. (The full-range of the Nyquist plots is in Fig. S1, ESI†). Typically, the intercept on the real axis is attributed to the series resistance (R_s). The left semicircle is assigned to the resistance capacitance (RC) network of the electrode/electrolyte interface, including the charge transfer resistance (R_{ct}) and the corresponding capacitance (C_μ). The right semicircle is assigned to the diffusion resistance (Z_N) of the redox couple in the electrolyte. The summary of the EIS data is shown in Table 1. The R_{ct} values of MoS_2 and WS_2 are both lower than 1 Ω (0.5 Ω, 0.3 Ω), indicating that MoS_2 and WS_2 are as effective as Pt for catalyzing triiodide reduction.[10] In addition, the large C_μ values of the two sulfide electrodes correspond to a large specific surface area, which is a crucial factor for high catalytic activities.[26] The Z_N values (> 100 Ω) for triiodide on the sulfide electrodes are higher than that on the Pt electrode (9.5 Ω). Based on eqn (4), Z_N varies inversely with the diffusion coefficient of triiodide (D). A large Z_N can be attributed to a low D which induces a low limiting current density (J_{lim}) according to eqn (5). This was confirmed using the Tafel-polarization test, as shown below. Although MoS_2 and WS_2 generated low R_{ct} values, the large Z_N was a negative factor in achieving an excellent catalytic activity. In other words, the combined actions
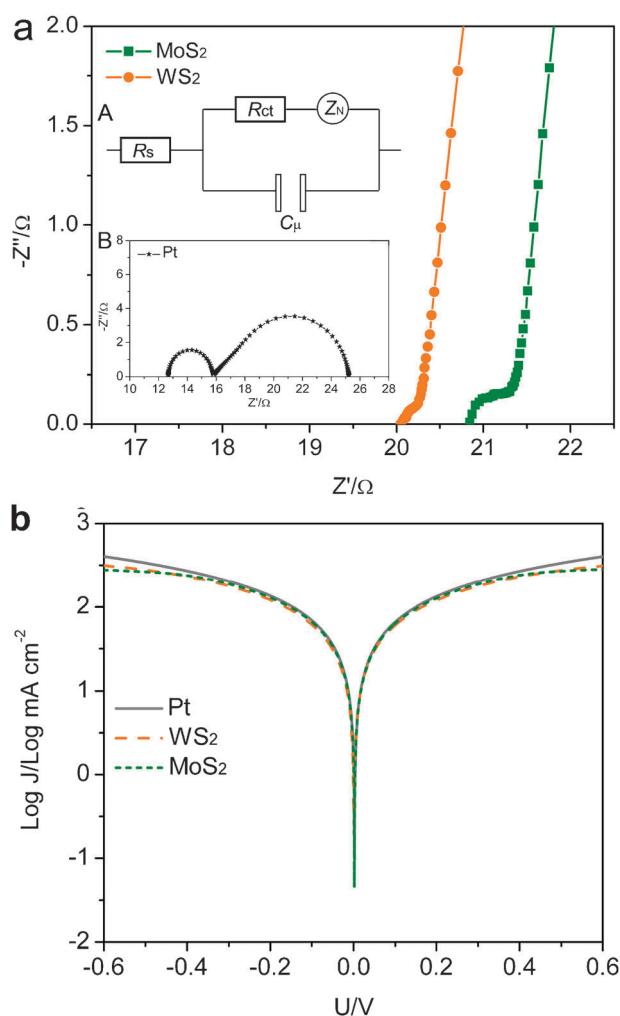
Fig. 4 (a) Nyquist plots of the symmetrical cells based on MoS_2 and WS_2 electrodes; (b) Tafel curve of the symmetrical cells based on MoS_2, WS_2, and Pt electrodes. Inset A in image (a): equivalent circuit diagram; inset B in image (a): Nyquist plot of the symmetrical cell based on Pt electrodes.

of R_{ct} and Z_N were responsible for the PCE values of the MoS_2-DSC and WS_2-DSC.

$$Z_N = \frac{W}{\sqrt{i\omega}} \tanh\left(\sqrt{\frac{i\omega}{K_N}}\right) \qquad (4)$$

where $W = kT/n^2e^2CA\sqrt{D}$; $K_N = D/\delta^2$, D is the diffusion coefficient of triiodide, C is the concentration of triiodide, n is the number of electrons transferred in the reaction, k is the Boltzmann constant, e is the elementary charge, and δ is the thickness of the diffusion layer.

$$J_{lim} = \frac{2neDCN_A}{l} \qquad (5)$$

where l is the spacer thickness, N_A is the Avogadro constant; and D, C, e and n have their usual meanings.

To verify the catalytic activities of MoS_2 and WS_2, Tafel-polarization measurements were performed using SCs similar to the cells used in the EIS test. Fig. 4b shows that Log J is a function of the potential (U). Compared with the Pt curve, the MoS_2 and WS_2 curves show a large slope indicating the

occurrence of a large exchange current density on the electrode surfaces. This implies high catalytic activity for the sulfide electrodes. In addition, the J_{lim} values of MoS_2 and WS_2 are lower than that of Pt. Based on eqn (4) and eqn (5), the Z_N values of MoS_2 and WS_2 are larger than that of Pt, which is in good accordance with the EIS results.

Finally, we attempted to use the two sulfide CEs for the regeneration of an organic redox couple, T_2/T^- (see ESI†, Fig. S2). The J–V curves of the DSCs using sulfide CEs and T_2/T^- electrolyte are available in Fig. S3, ESI.† The photovoltaic parameters for the DSC using a Pt CE are $V_{oc} = 0.63$ V, $J_{sc} = 12.23$ mA cm^{-2}, FF = 0.48, and $\eta = 3.70\%$. For the MoS_2 CE, the photovoltaic parameters are $V_{oc} = 0.63$ V, $J_{sc} = 12.52$ mA cm^{-2}, FF = 0.63 and $\eta = 4.97\%$. For the WS_2 CE, the photovoltaic parameters are $V_{oc} = 0.64$ mV, $J_{sc} = 12.99$ mA cm^{-2}, FF = 0.64, and $\eta = 5.24\%$. These represent improvements of 36% and 41% in the photovoltaic performances as compared to Pt. The V_{oc} values of the DSCs using the T_2/T^- redox couple are lower than those of DSCs using the I_3^-/I^- redox couple. This is consistent with the results obtained in a previous work.[27] The results prove that MoS_2 and WS_2 are more effective than Pt in the regeneration of the T_2/T^- redox couple. Thus, in the process of developing low-cost and highly efficient DSCs, the accouplement of the CE catalysts and the redox couples should be considered.

In summary, MoS_2 and WS_2 were introduced into DSCs system as counter electrode catalysts for the first time. The results show that the two sulfides hold excellent catalytic activities for regeneration of both the conventional redox couple (I_3^-/I^-) and a new organic redox couple (T_2/T^-). The I_3^-/I^- based DSCs using MoS_2 and WS_2 CEs achieved high power conversion efficiencies of 7.59% and 7.73%, respectively, which are close to the photovoltaic performance of the DSC using Pt CE. Furthermore, the T_2/T^- based DSCs using MoS_2 and WS_2 showed obvious improvements in PCE as compared to the DSC using a Pt CE. MoS_2 and WS_2 are promising counter electrode catalysts for low-cost and highly efficient DSCs.

Acknowledgements

Notes and references

1 M. Grätzel, *Nature*, 2001, **414**, 338.
2 A. Hagfeldt, G. Boschloo, L. Sun, L. Kloo and H. Pettersson, *Chem. Rev.*, 2010, **110**, 6595.
3 N. Cai, S.-J. Moon, L. Cevey-Ha, T. Moehl, R. Humphry-Baker, P. Wang, S. M. Zakeeruddin and M. Grätzel, *Nano Lett.*, 2011, **11**, 1452.
4 D.-H. Kim, J.-H. Heo, D.-J. Kwak and Y.-M. Sung, *J. Electr. Eng. Technol.*, 2010, **5**, 146.
5 A. Kay and M. Grätzel, *Sol. Energy Mater. Sol. Cells*, 1996, **44**, 99.
6 M. X. Wu, X. Lin, T. H. Wang, J. S. Qiu and T. L. Ma, *Energy Environ. Sci.*, 2011, **4**, 2308.
7 J. H. Wu, Q. H. Li, L. Q. Fan, Z. Lan, P. J. Li, J. M. Lin and S. C. Hao, *J. Power Sources*, 2008, **181**, 172.
8 Q. Tai, B. Chen, F. Guo, S. Xu, H. Hu, B. Sebo and X.-Z. Zhao, *ACS Nano*, 2011, **5**, 3795.
9 M. K. Wang, A. M. Angel, B. Marsan, N. C. Ha, N. Pootrakulchote, S. M. Zakeeruddin and M. Grätzel, *J. Am. Chem. Soc.*, 2009, **131**, 15976.

10 Q. W. Jiang, G. R. Li and X. P. Gao, *Chem. Commun.*, 2009, 6720.
11 Q. W. Jiang, G. R. Li, S. Liu and X. P. Gao, *J. Phys. Chem. C*, 2010, **114**, 13397.
12 H. Sun, D. Qin, S. Huang, X. Guo, D. Li, Y. Luo and Q. B. Meng, *Energy Environ. Sci.*, 2011, **4**, 2630.
13 M. X. Wu, X. Lin, A. Hagfldt and T. L Ma, *Angew. Chem., Int. Ed.*, 2011, **50**, 3520.
14 J. Jang, D. Ham, E. Ramasamy, J. Lee and J. S. Lee, *Chem. Commun.*, 2010, **46**, 8600.
15 M. X. Wu, X. Lin, A. Hagfeldt and T. L. Ma, *Chem. Commun.*, 2011, **47**, 4535.
16 M. X. Wu, Q. Y. Zhang, J. Q. Xiao, C. Y. Ma, X. Lin, C. Y. Miao, Y. J. He, Y. R. Gao, A. Hagfldt and T. L. Ma, *J. Mater. Chem.*, 2011, **21**, 20761.
17 L. Wang, M. X. Wu and T. L. Ma, *Appl. Phys. Lett.*, 2011, **98**, 221102.
18 L. Rapoport, Y. Bilik, Y. Feldman, M. Homyonfer, S. R. Cohen and R. Tenne, *Nature*, 1997, **387**, 791.
19 P. R. Bonneau, R. F. Jarvis Jr and R. B. Kaner, *Nature*, 1991, **349**, 510.
20 J. Bonde, P. G. Moses, T. F. Jaramillo, J. K. Nørskov and I. Chorkendorff, *Faraday Discuss.*, 2008, **140**, 219.
21 C. Lee, Q. Li, W. Kalb, X.-Z. Liu, H. Berger, R. W. Carpick and J. Hone, *Science*, 2010, **328**, 76.
22 T. F. Jaramillo, K. P. Jørgensen, J. Bonde, J. H. Nielsen, S. Horch and I. Chorkendorff, *Science*, 2007, **317**, 100.
23 K. Imoto, K. Takahashi, T. Yamaguchi, T. Komura, J.-I. Nakamura and K. Murata, *Sol. Energy Mater. Sol. Cells*, 2003, **79**, 459.
24 S. Biallozor and A. Kupniewska, *Electrochem. Commun.*, 2000, **2**, 480.
25 Y. Saito, W. Kubo, T. Kitamura, Y. Wada and S. Yanagida, *J. Photochem. Photobiol. A*, 2004, **164**, 153.
26 A. Hanch and A. Georg, *Electrochim. Acta*, 2001, **46**, 3457.
27 M. K. Wang, N. Chamberland, J. Breau, J.-E. Moser, R. Humphry-Baker, B. Marsan, S. M. Zakeeruddin and M. Grätzel, *Nat. Chem.*, 2010, **2**, 385.